

# Collective dynamics in coupled maps on a lattice with quenched disorder

Achille Giacometti <sup>(1)</sup>, Maurice Rossi <sup>(2)</sup>, and Libero Battiston <sup>(3)</sup>

<sup>(1)</sup> *INFM Unitá di Venezia, Dipartimento di Chimica Fisica, Università di Venezia, Calle Larga Santa Marta DD 2137, I-30123 Venezia-Italy*

<sup>(2)</sup> *Laboratoire de Modélisation en Mécanique CNRS Université Pierre et Marie Curie 4, Place Jussieu, 75005 Paris and*

<sup>(3)</sup> *ISAC CNR , Bologna, Unitá staccata di Padova Corso Stati Uniti 4, 35100 Padova*

(Dated: July 14, 2018)

It is investigated how a spatial quenched disorder modifies the dynamics of coupled map lattices. The disorder is introduced via the presence or absence of coupling terms among lattice sites. Two nonlinear maps have been considered embodying two paradigmatic dynamics. The Miller and Huse map can be associated with an Ising-like dynamics, whereas the logistic coupled maps is a prototype of a non trivial collective dynamics. Various indicators quantifying the overall behavior, demonstrates that even a small amount of spatial disorder is capable to alter the dynamics found for purely ordered cases.

PACS numbers: 05.45.Ra, 05.50.+q, 61.43.-j

Keywords:

## I. INTRODUCTION

Far-from-equilibrium systems, in which the simultaneous presence of non-linear terms and spatial extent is an essential feature, involve many important physical or chemical phenomena as varied as Rayleigh-Bénard convection in large horizontal boxes [1], chemical reaction-diffusion systems [2], colonies of micro-organisms [3] and fibrillating heart tissue [4]. In all these examples, the spatio-temporal chaos arising from the coupling of a large number of degree of freedoms, poses challenging theoretical questions which has so far eluded a universally accepted description. Progresses have often been limited to models containing the essential ingredients of typical extended systems at the crudest possible level. In this respect, "simple" partial differential equations such as, the Kuramoto-Shivashinsky, Ginzburg-Landau and Swift-Hohenberg equations, have proven to be useful models to identify main characteristics such as symmetry breaking, phase transition, phase dynamics, spatial chaos or defects. From a numerical point of view, however, these approaches, albeit successful, are rather demanding in terms of computational time. Coupled map lattices (CML) [5], where time and space are discretized from the outset, provide an alternative computational fast tool to study dynamical processes in spatially distributed systems. As the coupling with nearest-neighbours mimics the diffusion process, CML may be reckoned as a non-linear version of the diffusion process on a lattice. As a matter of fact, it is the subtle balance between diffusion and nonlinear effects that leads to the patterns and non-trivial time behaviors found in CML.

Pure diffusion on lattices has a long and venerable tradition in statistical mechanics [6]. It was originally motivated by solid-state applications as toy models for particle transport in ordered and disordered solids, but it has soon grown into a field in its own right. Interesting issues arise when a quenched disorder is introduced to model the fact that real life diffusion occurs in disordered media such as a porous medium (see e.g. [6] for a review). The presence of disorder drastically modifies the diffusion properties, sometime in a somewhat unexpected way [7]. Depending on its type and its strength, the disorder either inhibits diffusion (subdiffusion process) or enhances it by creating privileged paths (superdiffusion). Motivated by this scenario, the natural question arises of what would happen for CML in the presence of a quenched disorder, where three different mechanisms (non-linearities, diffusion and disorder) compete against one-another. This issue has already been addressed

for various non-linear systems [8]. Stochastically induced synchronization driven by the presence of additive noise has also been observed in spatially extended systems [9].

Clearly the presence of disorder induces a translational invariance breaking which generates a particular case of a system with a large number of degrees of freedom which are non equivalent. In analogy to what is observed in other problems of statistical physics, new phenomena may arise. As a matter of fact, aging, dynamical phase transition, anomalous transport have been observed in one-dimensional maps [8].

In the present paper, we focus on two-dimensional CML. Two such systems are investigated. On the regular lattice, the first one displays phase transitions (“ferromagnetic ordering”) and, the second one, a non-trivial global dynamics. Disorder is introduced at the simplest possible level, namely a prescribed fraction of bonds are randomly disconnected. This affects the phase diagram of the system : even a tiny fraction of disconnected bonds markedly modifies or destroys altogether, the dynamics found in the ordered lattice case.

The paper is organized as follows. In Sect. II, we briefly review some results on diffusion on a lattice and nonlinear coupled maps, while Sect.III introduces the way disorder is implemented in the lattice. Sect.IV details the numerical results for both CML models studied and Sect.V is devoted to some concluding remarks.

## II. DIFFUSION AND COUPLED MAPS ON A LATTICE

The most general master equation governing the linear diffusion of particles on a lattice reads

$$\partial_t P_{x_0x}(t) = \sum_{y(x)} [W_{xy}P_{x_0y}(t) - W_{yx}P_{x_0x}(t)] \quad (1)$$

where  $P_{x_0x}(t)$  stands for the probability of being at site  $x \in \mathcal{Z}^d$  of a hypercubic lattice of dimension  $d$ , having started at site  $x_0$  at the initial time  $t_0 = 0$ .  $W_{xy}$  denotes the transition rate for a jump  $y \rightarrow x$  and is different from zero only for nearest-neighbours  $y$  of site  $x$  (the notation  $y(x)$  in the sum reflects this constraint). A time discretized version (in time units such that  $\Delta t = 1$ ) reads

$$P_{x_0x}(t+1) = (1 - \epsilon_x)P_{x_0x}(t) + \sum_{y(x)} W_{xy}P_{x_0y}(t) \quad \text{where} \quad \epsilon_x = \sum_{y(x)} W_{yx} \quad (2)$$

If only positive symmetric transition rates  $0 \leq W_{xy} = W_{yx}$  are allowed and  $\sum_{y(x)} W_{xy} = 1$  (for all  $x$ ), then one easily verifies that (a)  $0 \leq P_{x_o x}(t) \leq 1$  and (b) the total probability is conserved. The physical process associated to such a mathematical framework can be described as follows : at each time  $t$  a particle at  $x$  can either move to a nearest-neighbour  $y(x)$  with rate  $W_{yx}$  or stay at  $x$  with probability  $1 - \epsilon_x$ . Quantities  $W_{xy}$  are generally random with the *proviso* that condition  $0 \leq \epsilon_x \leq 1$  should hold true for any  $x$ . Standard diffusion corresponds to  $W_{xy} = 1/z$  where  $z = 2d$  denotes the coordination number of a d-dimensional hypercubic lattice. Introducing a quenched disorder in the transition rates  $W_{xy}$  changes the classical diffusion behavior into a sub-diffusive or super-diffusive one [7]. Such a toy model may be used to understand a variety of complex systems such as optical excitation, polymers and diffusion-limited binary reaction [6].

Other interesting dynamical features arise when non-linear terms are introduced in the local dynamics. Let  $C_x(t)$  be a real variable defined at point  $x$  and time  $t$ . This quantity belongs to the interval  $[-1, 1]$  and satisfies

$$C_x(t+1) = (1 - zg)F[C_x(t)] + g \sum_{y(x)} F[C_y(t)] \quad (3)$$

in which  $F(C)$  stands for a non-linear homomorphism in  $[-1, 1]$ . Quantity  $C_x(t)$  may represent the concentration of a binary mixture, the values  $-1$  and  $+1$  corresponding to a pure phase of the first or second component respectively. The above equation resembles equation (2) with  $W_{xy} = g$  for all nearest-neighbours but with a non-linear map  $F(C)$ . Coupling  $g$  between neighbour sites is constrained to satisfy  $0 \leq g \leq 1/2d$  so that, if the initial concentration is in the range  $[-1, 1]$ , it remains within the same interval for all times. The first r.h.s factor in equation (3) accounts for the “self-interaction” term, that is the coupling of each site with itself. As  $g \rightarrow 0^+$ , each site evolves independently of the other (“high temperature regime”). At  $g = 1/(2d + 1)$ , each site is coupled with all its nearest-neighbours as well as with itself in an identical manner (“democratic coupling”). Finally as  $g \rightarrow g_{max} = 1/2d$ , the self-interaction term vanishes and all nearest-neighbour sites are strongly and equally coupled (“low temperature regime”). For a two-dimensional lattice, the democratic coupling and the low-temperature regime correspond to  $g = 0.2$  and  $g = 0.25$  respectively.

In the present work, we consider a finite size lattice consisting of  $L$  sites along each spatial direction with standard periodic boundary conditions. Two maps  $F(C)$  are studied, each one

representing a particular class of dynamics. The first one is the Miller and Huse map [10] [11]

$$F_\mu(C) = \begin{cases} -2\mu/3 - \mu C & \text{for } -1 < C < -1/3 \\ \mu C & \text{for } -1/3 < C < 1/3 \\ 2\mu/3 - \mu C & \text{for } 1/3 < C < 1 \end{cases} \quad (4)$$

where  $C \in [-1, 1]$ . The map (4) with  $\mu = 3$  was introduced by Miller and Huse to mimic a statistical system having two equilibrium states i.e. a Ising-like dynamics. This model is appropriate to describe a spinodal decomposition mechanism if variable  $\sigma_x(t) \equiv \text{sign}[C_x(t)] = \pm 1$  plays the role of an Ising spin. In that case, a magnetization can be defined as follows:

$$m(t) = \frac{1}{V} \sum_x \sigma_x(t) \quad (5)$$

where  $V = L^d$  is the total number of sites.

The second study concerns the logistic map

$$F_\mu(C) = 1 - \mu C^2 \quad 0 \leq \mu \leq 2 \quad C \in [-1, 1]. \quad (6)$$

This CML possesses a number of interesting dynamical features [11]. In particular, the spatially averaged quantity

$$\overline{C(t)} = \frac{1}{V} \sum_x C_x(t) \quad (7)$$

possesses a macroscopic time-periodic evolution while spatial patterns similar to those found for Miller-Huse map are not visible. Moreover the graph of the asymptotic time evolution of  $\overline{C(t)}$ , with respect to parameter  $\mu$  displays a bifurcation diagram similar to the one observed for a unique Logistic map [12].

### III. COUPLED MAP LATTICE AND DISORDER.

In close analogy with linear diffusion on a lattice, the effect of a quenched disorder is introduced on the two CML discussed above. The generalization of Eq.(3) then reads

$$C_x(t+1) = (1 - \epsilon_x)F[C_x(t)] + \sum_{y(x)} W_{xy}F[C_y(t)] \quad (8)$$

Paralleling the diffusion case, couplings are partially random and verify for arbitrary  $x$

$$W_{yx} = W_{xy}, \quad 0 < \epsilon_x \equiv \sum_{y(x)} W_{yx} \leq 1. \quad (9)$$

As a consequence, quantities  $C_x(t)$  always remain within the original interval  $[-1, 1]$  since

$$|C_x(t+1)| \leq (1 - \epsilon_x) + \sum_{y(x)} W_{xy} \leq (1 - \epsilon_x) + \sum_{y(x)} W_{yx} = 1. \quad (10)$$

This model includes all the previous cases:

- a) Linear diffusion with disorder (2) when  $F(x) \equiv x$ .
- b) Nonlinear coupled maps (3) when  $W_{xy} = g$  (and hence  $\epsilon_x = zg$ ).

In the following, a quenched binary disorder is used satisfying the distribution

$$\rho(w) = (1 - p) \delta(w - g) + p\delta(w) \quad (11)$$

where  $p$  stands for the percentage of connections which are cut. The value  $p = 0$  corresponds to the regular case. It should be emphasized that, as bonds are removed, the self-interaction term increases (see Eq.(8)). Disorder may set a competitive mechanism disfavoring the balance involving couplings between lattice points, which tends to "synchronize" the maps spatially or temporally and the non-linearity of the maps, which tend to destabilize them. Disorder is thus expected to act as a further destabilization preventing the onset of an "ordered" phase.

#### IV. NUMERICAL RESULTS

Numerical results are obtained on a square lattice ( $d = 2$ ). The Miller and Huse case is first presented in Sect. A,B,C as a prototype of a spinodal decomposition mechanism. Sect. D and E are devoted to the logistic map where a global time evolution is observed.

##### A. The ordered Miller and Huse phase diagram for $\mu = 3$ and $\mu = 1.9$

Fig.1 (top) depicts the Miller-Huse phase diagram for  $\mu = 3$  [10]. If  $m^2$  denotes the value of the mean-square magnetization, this quantity is raised to two suitable exponents  $\langle m^2 \rangle^{\frac{1}{2\beta}}$  and

$\langle L^2 m^2 \rangle^{-\frac{1}{\gamma}}$ , and plotted as a function of the coupling strength  $g$ . In their original paper, Miller and Huse used the two dimensional Ising critical exponents  $\beta_{Ising} = 1/8$  and  $\gamma_{Ising} = 7/4$  [13]. A successive and more refined work [14] identified the characteristics exponents values  $\beta \sim 0.111$ ,  $\gamma \sim 1.55$  which are close but not identical to those of the two dimensional Ising model. Figure 1 was obtained for lattice size  $L = 128$  with a magnetization which was computed after  $T = 2 \times 10^5$  iterations which appear to be large enough to reach a steady state, and averaged over 10–50 different initial conditions (50 refers to the left branch of the phase diagram  $g \leq g_c$ , where fluctuations are much higher). As one approaches the critical value  $g_c = 0.20(5)$ , a phase transition occurs. This result is in agreement with those of [14] which pinned down the transition value at  $g_c = 0.2051(5)$  on the basis of more extensive simulations. Fig.1 (bottom) provides the same computations for  $\mu = 1.9$  and indicates a critical value  $g_c = 0.16(8)$  not previously reported. Here and below the parenthesis indicates the degree of uncertainty of the result.

The fact that the total magnetization is not conserved, suggests that this dynamics could be akin to a dynamical Ising model with non-conserved magnetization (model A)[16, 17]. However, the critical coupling, as well as the time evolution (see below)  $g_c$  changes for different  $\mu$ . This feature is apparent in Fig. 2 where, starting from a random and uncorrelated initial condition for  $g > g_c(\mu)$ , two snapshots are depicted for  $\mu = 3$  (top) and  $\mu = 1.9$  (bottom) at stages  $t = 100$  (left) and  $t = 1000$  (right).

## B. The persistence probability in the case of a regular lattice

Another interesting quantity, is the persistence probability  $P_s(t)$ , which measures the fraction of spins which have not changed sign up to time  $t$ . This concept was first introduced within this context in [11]. It was shown that, for  $\mu = 1.9$ , a transition occurs at  $g_e \sim 0.169$  appearing as an abrupt modification in the slope of probability  $P_s(t)$  (Fig 3). For  $g_e \leq g$ , this probability takes the form

$$P_s(t) \sim t^{-\theta} \quad \text{with} \quad \theta(g) \sim (g - g_e)^w \quad (12)$$

Values  $w \sim 0.20$  and  $g_e = 0.16(9)$  are reported in [11]. This latter number is strikingly close to the critical value  $g_c = 0.16(8)$  found in the above section. The transition of the persistence probability thus appears to be a consequence of the phase transition of magnetization (and

not computed in [11]), rather than a different transition.

### C. Miller-Huse coupled map lattice with binary quenched disorder

Let us now introduce a slight disorder on the Miller and Huse coupled maps. Two small percentages of disconnected bonds have been used :  $p = 0.05$  and  $p = 0.065$ . Results for  $\mu = 3$  are reported in Fig. 4. Note that exponents of the undiluted case are employed on the basis that critical exponents of the Ising model with random binary coupling are found to be similar to those computed for a regular lattice [18]. Dilution has the effect of shifting the critical coupling  $g_c$  to higher values. This shift can be qualitatively understood by a simple argument. Let denote  $z(p) = z(1-p)$  the average effective coordination number with dilution  $p$ . Within a mean field description, the average coupling strength increases in the presence of dilution by a factor

$$\frac{g_c(p)}{g_c(p=0)} = \frac{1}{1-p} \quad (13)$$

thus leading to a linear dependence for  $g_c(p)$  for small values of  $p$ . Our calculations reproduce this linear behavior (Fig. 5), although with a different numerical value of slope.

As the maximum possible  $g$  is equal to a constant  $g_{\max} = 1/2d = 0.25$ , the right branch of the phase diagram shrinks as  $p$  increases, and there will be a critical threshold  $p_c$ , such that  $g(p_c) = g_{\max}$ , above which a phase transition is no longer observed. Results of Fig.5 then suggest  $p_c \sim 0.11$ , although a more extensive analysis would be needed for a precise estimate.

We checked that, for values  $p > p_c$ , the ferromagnetic transition is indeed not observed. A small percentage of disconnected bonds therefore disfavours a collective behavior and can even inhibit the transition. A similar trend is mirrored by the persistence probability (Fig. 6), which is computed with a dilution  $p = 0.05$  and under the same conditions as in Fig. 3. This also supports the equivalence between persistence and ferromagnetic transitions.

Patterns for both  $\mu = 3$  and  $\mu = 1.9$  above the critical coupling ( $g > g_c(\mu)$ ) are shown at some intermediate time ( $t = 1000$ ) in Fig. 7 for dilution  $p = 0.05$ . These are the analogous of those previously obtained under the same conditions in the regular lattice (Fig. 2). If patterns are pinned by defects, we expect similar patterns upon a rescaling conserving the quantity  $pL^2$ . Indeed, the number of "defects" (sites with disconnected bonds) should be equal to the fraction  $p$  of disconnected bonds times the total surface  $N \equiv L^2$ . Figure 8



indicates that this is precisely the case as the patterns obtained at a relatively late stage of the evolution ( $t = 10^4$ )  $L = 128, p = 0.05$ , and  $L = 256, p = 0.0125$ ,  $L = 512, p = 0.003125$  are quite similar.

#### D. The Logistic CML and non-trivial collective behavior

In the Miller-Huse CML, the emphasis was on collective spatial behavior in the sense of ordinary critical phenomena. By contrast, the logistic CML (6) is an example of a collective time evolution [11]. Depending on parameter  $\mu \in [0, 2]$ , a large variety of complex behaviors are observed. Building upon previous analyses on this system with no disorder [11], an extensive analysis is performed both with and without disorder. Our results are in perfect agreement with published results [11] [12]. In addition, we address issues such as transient behavior, coupling dependence and competition with disorder, that were not previously covered.

System (3) is first iterated for extremely long time and spatial average  $\overline{C(t)}$  is thereafter computed when a steady state is expected to be attained. Note that some numerical tests require times up to  $T = 5 \times 10^6$  which would be prohibitively long for size  $L = 2048$ . Hence our investigations have been performed with smaller sizes ( $L = 1024, L = 128$  and  $L = 64$ ). This steady state condition is checked for by considering  $\overline{C(t)}$  at several successive large times and showing that the same sequence is periodically found. This sequence is then analyzed as a function of parameter  $\mu$  for different couplings  $g$ . For democratic coupling  $g = 0.2$ , a highly regular time evolution arises yielding a periodic doubling bifurcation cascade for  $\overline{C(t)}$ . Fig. 9 reports results for two computations:  $L = 128$  with  $T = 10^6$ , and  $L = 1024$  with  $T = 10^4$ . Both results nicely superimpose and are compatible with those of [11] [12] up to fluctuations of order  $1/\sqrt{L}$  (in these work, a size  $L = 2048$  was used). This suggests that the CML behaves in the thermodynamic limit and that steady state has been reached in both cases. For other couplings, the observed behavior can be more involved. Indeed identical computations were repeated for weaker couplings ( $g = 0.1$  in Fig. 9). For  $L = 128$ , the same final time is used, and quite a few "singular" points (i.e. outside the bifurcation diagram) are now distinguishable. For size  $L = 1024$ , computations have been performed up to times as large as  $10^4$  and the system is always found in a transient state (see last picture of Fig.9), in contrast with the  $L = 128$  case. As in the uncoupled case  $g = 0$ , values

of  $C_x(t)$  are almost uniformly distributed with the exception of some particular windows characteristic of the single map, it is then plausible to expect longer transient regimes and a stronger dependence on the initial conditions in the weak coupling regime ( $g < 0.2$ ). Indeed Fig. 10 shows snapshots of spins  $\sigma_x(t)$  (left) and fields  $C_x(t)$  (right) at two extremely long times ( $T$  and  $T + 1$  with  $T = 10^6$ ) for *identical parameters* ( $L = 64$ ,  $g = 0.1$ ,  $\mu = 1.66$ ). The two situations only differs by their *random* initial conditions. For the first initial conditions (first two rows), an oscillation is observed between two different states corresponding to the two branches of Figure 9. This is confirmed by the corresponding probability distribution function (PDF) in which a well defined bimodal character can be identified (Fig. 11 (a)). The second random initial condition leads to a different pattern (see the last two rows of Fig.10). The lattice is now divided into two regions. In each region, the system is behaving as before but there exists a relative phase lag between the two "sub-lattices". This feature is also visible in the PDF, of Fig.11 (b) where the new bimodal PDF is a linear combination of the previous two distributions. As a consequence, the value of  $\overline{C(t)}$  is shifted towards "singular" points reported in Fig.9. These "frozen" states have extremely long and possibly infinite relaxation times.

Upon identifying a suitable order parameter and monitoring the variation of such a parameter with coupling  $g$ , one finds a transition from a "high temperature" to a "low temperature" phase, akin to that found for the Miller-Huse map. A proper definition of the order parameter is, however, a delicate matter. Depending on the value of the coupling  $g$ , the spatial average  $\overline{C(t)}$  is a time constant or it follows a periodic sequence. Hence, by computing

$$\psi(t) = \left| \frac{\overline{C(t+1)} - \overline{C(t)}}{\overline{C_{ave}(t)}} \right| \quad \text{with} \quad \overline{C_{ave}(t)} = \frac{[\overline{C(t+1)} + \overline{C(t)}]}{2}. \quad (14)$$

for sufficiently long times, it is expected to get value of  $\psi(t \rightarrow \infty)$  close to 0 for small  $g$ , and a non-zero value for  $g \geq g_c$  [19]. An abrupt change is indeed observed (Fig. 12) for a given  $g_c(\mu)$ . For instance, one obtains  $g_c \sim 0.1$  for  $\mu = 1.7$ . More extensive and systematic calculations on this point are left for a future study.

### E. Effect of a binary quenched disorder on the logistic coupled map lattice.

Let us now consider the coupled logistic maps in the presence of binary quenched disorder. We find that even a small amount of disorder is sufficient to modify the "conventional"

pattern reported on the regular lattice, and this is true irrespective of sizes  $L$ . Moreover, long transients are now present even in the democratic coupling  $g = 0.2$ . For instance we have explicitly checked that, for  $L = 1024$ ,  $T = 10^4$  is no longer sufficient to reach the steady state. We hence consider size  $L = 128$  for which a sufficiently long time ( $T = 4.5 \times 10^6$ ) can be attained to ensure steady state conditions. Spatial average  $\overline{C(t)}$  is shown in figure 13 versus parameter  $\mu$ , for coupling  $g = 0.2$  and two weak dilutions  $p = 0.05$  and  $p = 0.1$ . Once a small fraction of the total number of bonds is missing, the formation of the period doubling sequence is shifted to the left : disorder thus tends to inhibit the formation of the bifurcation structure. An additional increase in the dilution  $p$  gives rise to a further shift to the left, and eventually to destruction of the collective dynamics for a sufficiently high  $p = p_c$ . This conclusion is supported by further calculations (not shown) on a smaller size ( $L = 64$ ) where a systematic trend to the left is observed as  $p$  increases. However, the large fluctuations present for such a small size prevent us from a quantitative measure of the critical threshold.

### F. The Lyapunov spectrum

As suggested in [20], the Lyapunov spectrum is *a priori* another useful quantity to analyze the collective behavior of CLM. The computation is performed by recasting Eq.(8) in the following form:

$$C_x(t+1) = \sum_y M_{xy} F[C_y(t)] \quad (15)$$

where the matrix  $M_{xy}$  stands for

$$M_{xy}(\{W\}) = (1 - \epsilon_x)\delta_{xy} + W_{xy}\delta_{|x-y|,1} \quad (16)$$

Upon considering a variation  $\delta C(t)$  of a given solution  $C^0(t)$ , one obtains

$$\delta C_x(t+1) = \sum_y M_{xy} F'[C_y^0(t)] \delta C_y(t) \quad (17)$$

The map enters into equation (17) only through the value  $F'[C^0]$ . The Lyapunov exponents are computed by taking into account the time evolution of an initially small variation  $\delta C_x(t = 0)$ . This procedure is standard and outlined in [21]. To compute the lower part of the spectrum with sufficient precision, the time window for the evolution is kept sufficiently

small and the number of time intervals for normalization is increased accordingly. This procedure has been applied for both the Miller-Huse and the logistic map. A cross-checking for the good performance of the algorithm can be carried out by computing the exact eigenvalues for the uncoupled case  $g = 0$  and the diffusion linear map. In this latter case, the eigenvalues of matrix  $M_{xy}$  are directly connected to the Lyapunov exponents.

In the regular case, the Lyapunov exponent spectrum has already been carried out for the Miller-Huse map at  $\mu = 3$  [20]. In that work, it was suggested that the Lyapunov spectrum is not sensitive to the presence of the “ferromagnetic ordering” discussed earlier. The independence of the spectrum on the critical coupling  $g_c$  was also related to the fact that chaotic fluctuations, as measured by the Lyapunov spectrum, have short range and thus decouple from the the long-range spatial effect giving rise to the ferromagnetic ordering at the critical coupling  $g_c$ . This result is confirmed by our computations which were carried out at various sizes (from  $L = 24$  as in [20] to  $L = 256$ ). Figure 14 plots the first 100 most unstable exponents (this represents a small fraction of the spectrum whose size is  $V = L^2 = 16384$  for  $L = 128$ ) versus the normalized index  $x = i/L^2$  for two values of the coupling (one below and the other above the critical coupling  $g_c \sim 0.205$ ). As in [20], no sign of transition can be traced in the results. The spectrum is continuous starting with a value which is well below the unique exponent of the uncoupled case  $\sim 0.9$ . The independence of these results for the upper spectrum on the size  $L$  of the system has been verified. The effect of the dilution on this spectrum has been analyzed in the presence of different degrees  $p$  of dilution. Fig. 14 displays the results for  $p = 0.1$  showing that disorder lowers the values of the Lyapunov spectrum.

For the logistic map, we are not aware of any previous calculations even in the regular case. Fig. 15 depicts our results both in the undiluted and the diluted case in the case of a democratic coupling  $g = 0.2$  and for two different values  $\mu = 1.85$  and  $\mu = 1.65$ . For the first  $\mu$  the spatial average  $\overline{C(t)}$  is a time constant, whereas for the second value of  $\mu$ ,  $\overline{C(t)}$  is time periodic. Nevertheless, no qualitative difference is found in the Lyapunov spectrum which is simply shifted to higher values as  $\mu$  increases. Unlike in the Miller-Huse case, the presence of disorder appears in the Lyapunov spectrum in the form of a gap separating the first few Lyapunov exponents from the rest of the spectrum (Fig. 15). Again, the effect of changing the value of the parameter  $\mu$  is a shifting of the numerical value of the exponents, in agreement with the undiluted case. On recalling the analogy between the Lyapunov

spectrum and the problem of the Schrödinger equation on a lattice [22], the emergence of the gap in the lowest part of the Lyapunov spectrum in the presence of “defects”, can be regarded as the analog of a “localization” mechanism. On the other hand this analogy is certainly limited, or it is at least incomplete, since it does not apply to the Miller and Huse case discussed earlier.

## V. CONCLUSION

We have shown that the phenomenology of spatio-temporal nonlinear systems may be significantly changed by a small amount of quenched disorder. This feature has been demonstrated on two-dimensional CML with periodic boundary conditions. Two paradigmatic cases have been investigated. The first one is the Miller and Huse case, which is known to display a phase transition in the strong coupling (low temperature) phase. The transition is found to be delayed and even inhibited by a small amount of binary noise. A percentage of disconnected bonds as small as 10% is sufficient to destroy the ordered phase. This feature is mirrored by an analogous transition on the persistence probability. The second paradigmatic case concerns the logistic map which exhibits a remarkable time evolution of the spatial average  $\overline{C(t)}$  on a regular lattice. In this case, issues regarding the possibility of long transient behaviors have been addressed. As it turns out, in the non-democratic case, the system might get trapped into a metastable state away from the expected bifurcation branch. In addition, the phase diagram  $\overline{C(t)}$  versus  $\mu$  is markedly affected (even in the democratic case) by a small percentage of dilution (e.g. 5%).

This work is believed to unravel some aspects of the interplay between quenched disorder and non-linear processes for cases which were not previously studied. In particular, it indicates that the lattice structure affects in a major way the system dynamics. Along this line of thought, it would be worth modifying the nature of the disorder to understand the significance of the qualitative nature of disorder. This can be done, on the one hand, by changing coupling amplitudes with position rather than by cutting some links as performed in the present paper, or, on the other hand, by considering topological disorder such as a fractal structure.

### Acknowledgments

Financial support from a CNR-CNRS exchange program is greatly acknowledged. We would like to thank A. Torcini for useful criticisms and suggestions as well as a careful reading of a first draft of the manuscript. We have also benefited from useful suggestions from R. Livi, A. Politi, P. Marq and P. Manneville.

- 
- [1] S.W. Morris, E. Bodenschatz, D. S. Cannel, G. Ahlers, Phys. Rev. Lett. **71**, 2026 (1993)
  - [2] Q. Ouyang and J. M. Flesselles, Nature **379**, 143 (1996)
  - [3] K. J. Lee, E. C. Cox, R. E. Goldstein, Phys. Rev. Lett. **76**, 1174 (1996)
  - [4] Z. L. Qu, J. N. Weiss, A. Gartfinkel, Phys. Rev. Lett. **78**, 1387 (1997)
  - [5] K. Kaneko ed. *Theory and Applications of Coupled Map Lattice* (Wiley, New York 1993)
  - [6] J. Haus and K. Kehr, Phys. Rep. **150**, 263 (1987); S. Havil and D. Ben-Avraham, Adv. Phys.**36**, 659 (1987); S. Alexander et al, Rev. Mod. Phys. **53**, 175 (1981); J. P. Bouchaud and A. Georges, Phys. Rep. **195**, 127 (1990)
  - [7] A. Giacometti and KPN Murthy, Phys. Rev. E **53**, 5647 (1996) and references therein.
  - [8] G. Radons, W. Just, P. Haüssler (edts) *Collective dynamics of non linear and disordered systems*.(Springer Verlag, 2004)
  - [9] L. Baroni, R. Livi and A. Torcini, Phys. Rev. E **63**, 0362226 (2001); L. Angelini, M. Pellicoro and S. Stramaglia, Phys. Lett. A **285**, 293 (2001)
  - [10] J. Miller and D.A. Huse, Phys. Rev. **A**, 2528 (1993)
  - [11] A. Lemaître and H. Chaté Phys. Rev. Lett. **82**, 1140 (1999)
  - [12] Anaël Lemaître, Ph.D thesis, École Polytechnique, France (1998)
  - [13] H.E. Stanley, "Introduction to Phase Transition and Critical Phenomena", Oxford University Press, New York 1971
  - [14] P. Marq, H. Chaté, and P. Manneville, Phys. Rev. E **55**, 2606 (1997)
  - [15] Alan Bray Adv. Phys. 43, 357 (1994)
  - [16] P. C. Hohenberg and B. I. Halperin Rev. Mod. Phys. 49, 435-479 (1977)
  - [17] J. Krug and H. Spohn in "Solids Far from Equilibrium", C. Godrèche ed., Cambridge University Press, Cambridge 1991 pp. 479

- [18] A. Roder, J. Adler and W. Janke, *Physica A* **265**, 28 (1999)
- [19] A similar line of reasoning has already been followed by P. Marq (private communication)
- [20] C. S. O'Hern, D. A. Egolf and H. S. Greenside, *Phys. Rev. E* **53**, 3374 (1996)
- [21] G. Benettin, L. Galgani, A. Giorgilli, J-M. Strelcyn *Meccanica* **15**, 9 (1980)
- [22] S. Isola, A. Politi, S. Ruffo, A. Torcini, *Phys. Lett. A* **143**, 365 (1990)

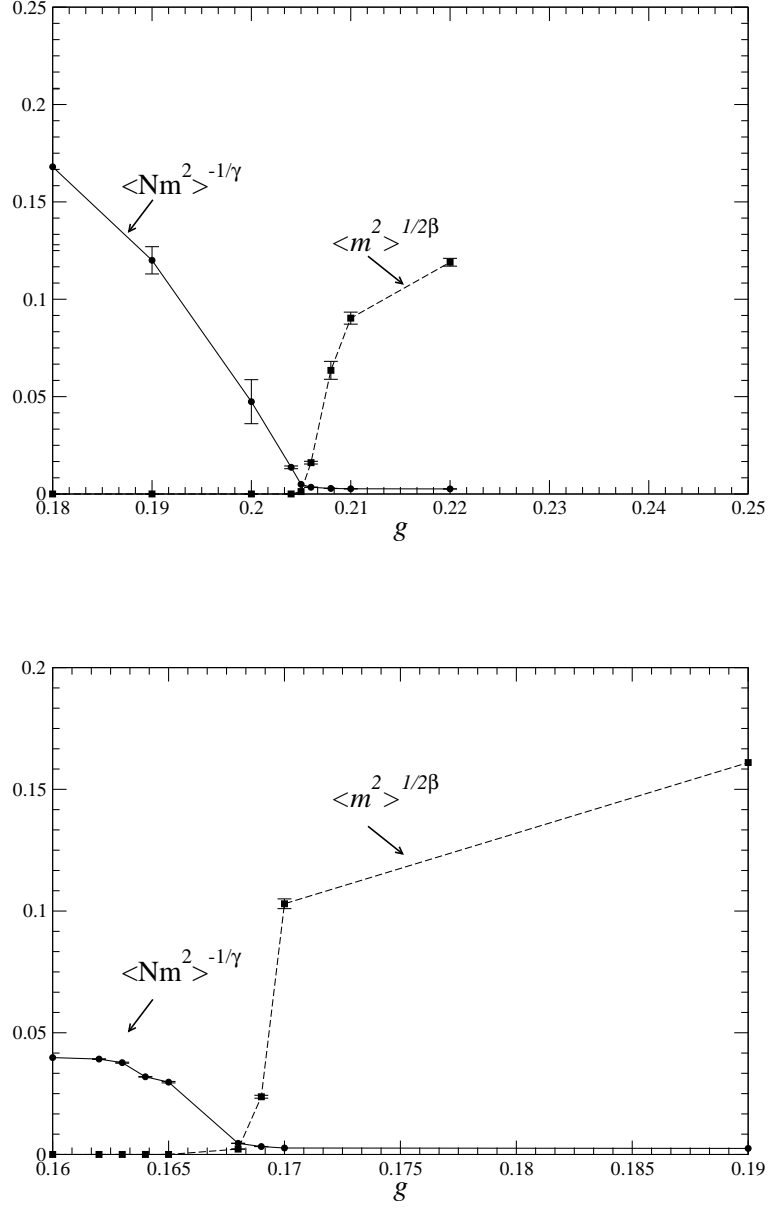


FIG. 1: The phase diagram for the Miller and Huse map for  $\mu = 3$  (top) and  $\mu = 1.9$  (bottom). The lattice sites are  $N = L \times L$  with  $L = 128$  and magnetization is computed once  $T = 2 \times 10^5$  iterations have been performed and exponents  $\gamma$  and  $\beta$  are those identified in [14].



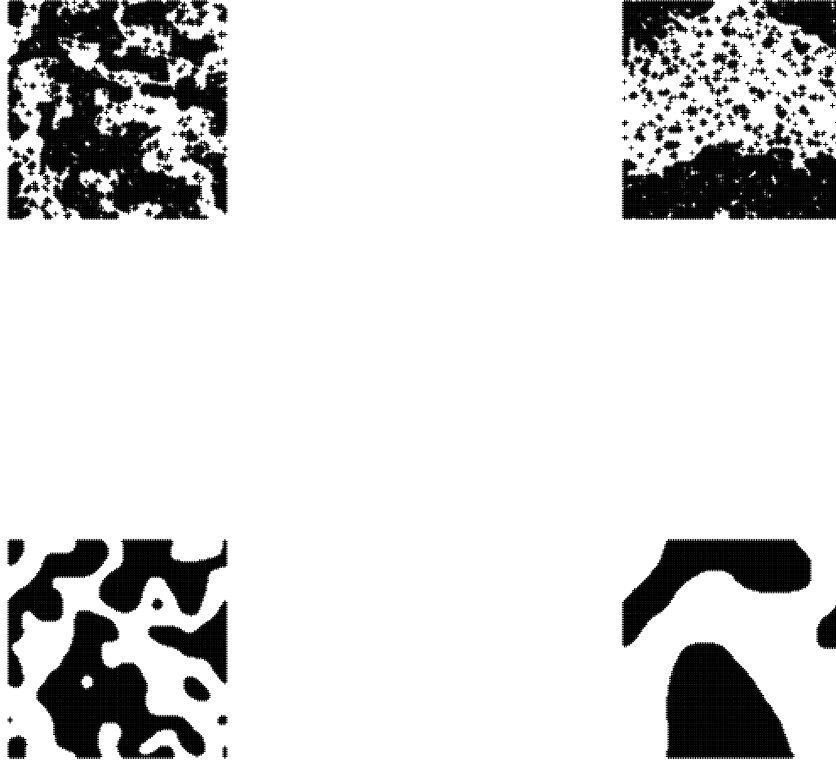


FIG. 2: Snapshots for the Miller and Huse CML on the regular lattice for  $g > g_c$ . Case  $\mu = 3$ ,  $g = 0.21$  (top) with  $t = 100$  (left),  $t = 1000$  (right). Case  $\mu = 1.9$ ,  $g = 0.20$  (bottom) with  $t = 100$  (left),  $t = 1000$  (right). The lattice size is  $L = 128$ .

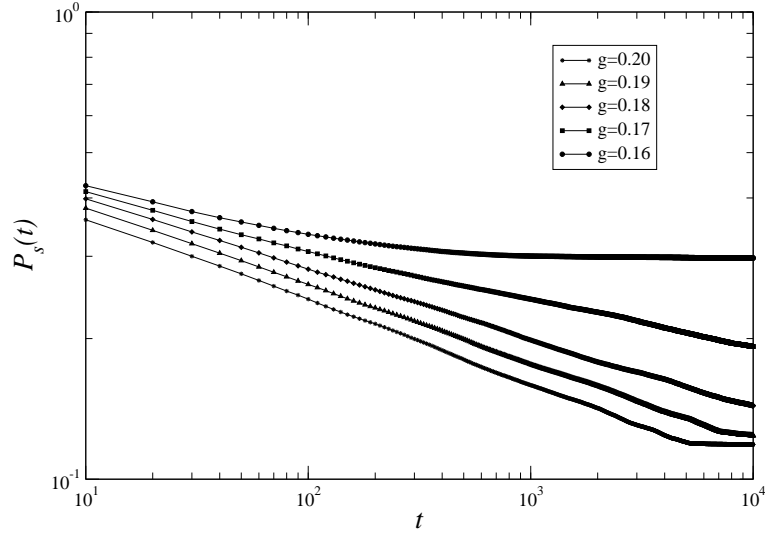


FIG. 3: The persistence probability for the Miller and Huse maps on the regular lattice for  $\mu = 1.9$  ( $g = 0.16$  is the uppermost curve). The lattice size is  $L = 128$ .

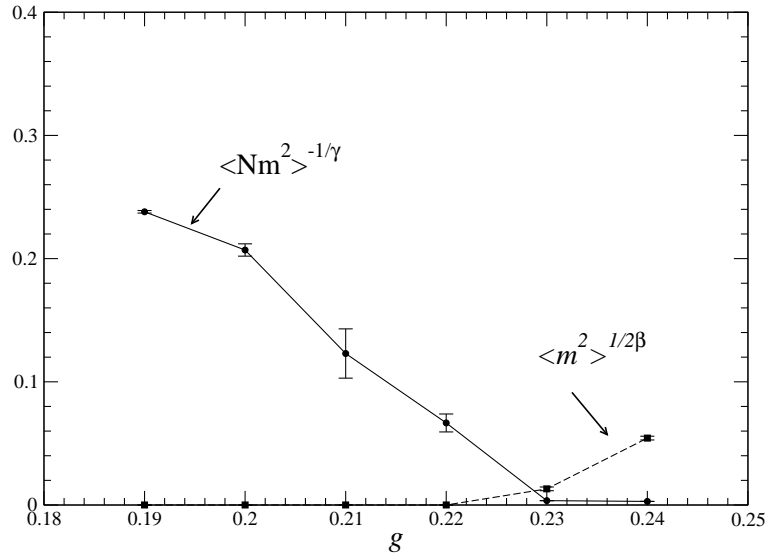
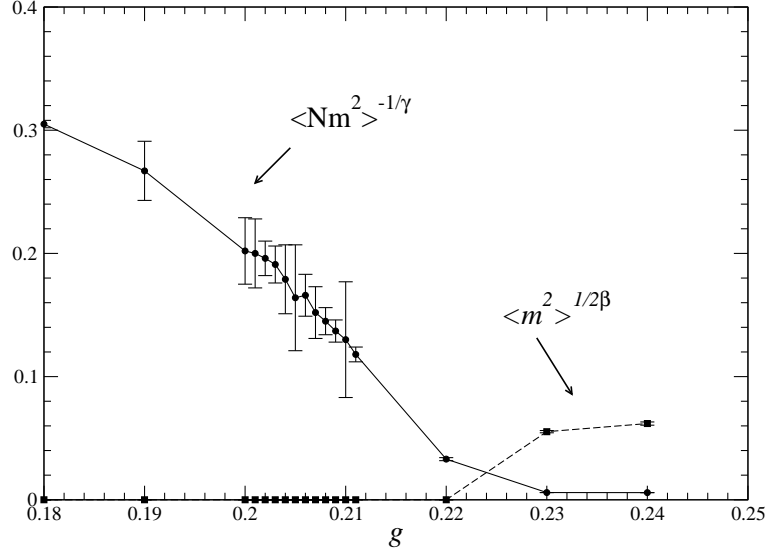


FIG. 4: Phase diagram for Miller and Huse maps for  $\mu = 3$  and dilution:  $p = 0.05$  (top) and  $p = 0.065$  (bottom). Lattice size is  $L = 128$ . Magnetization is computed once  $T = 2 \times 10^5$  iterations have been performed and exponents  $\gamma$  and  $\beta$  are those identified in [14].

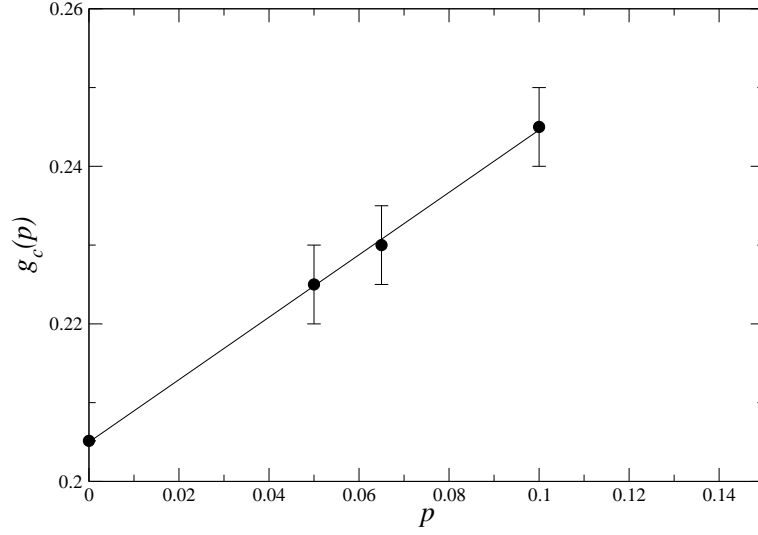


FIG. 5: Critical coupling  $g_c$  as a function of the dilution parameter  $p$ . Miller-Huse model for  $\mu = 3$ . The solid line represents a best fit result yielding  $p_c \sim 0.11$  for  $g_c = 0.25$ .

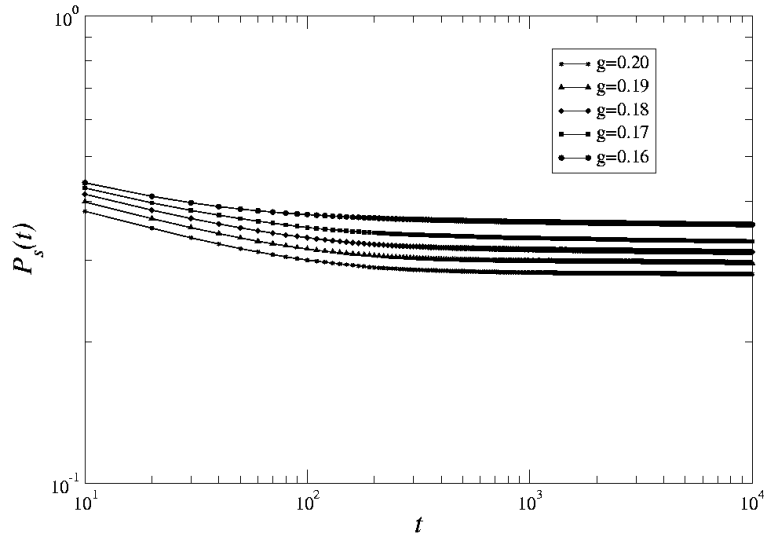


FIG. 6: Persistence for the Miller and Huse map for  $\mu = 1.9$  and dilution  $p = 0.05$ .

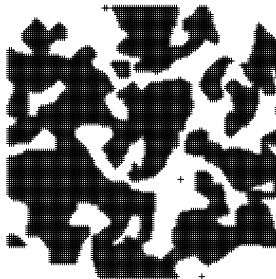
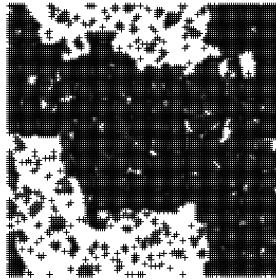


FIG. 7: Snapshots for the Miller and Huse map with dilution ( $p = 0.05$ ) for  $g > g_c(p)$  in the case  $\mu = 3$ ,  $g = 0.23$ ,  $t = 1000$  (top), and in the case  $\mu = 1.9$ ,  $g = 0.20$ ,  $t = 1000$  (bottom). Here the size is  $L = 128$ .

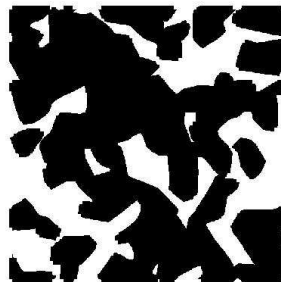
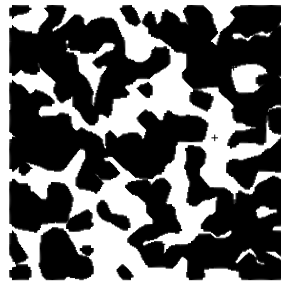
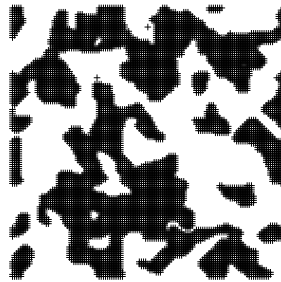


FIG. 8: Various rescaled patterns at different  $p$  but constant  $pL^2$ . Parameters are  $g = 0.2$  and  $\mu = 1.9$ . From top to bottom,  $L = 128$  and  $p = 0.05$ ;  $L = 256$  and  $p = 0.0125$ ;  $L = 512$  and

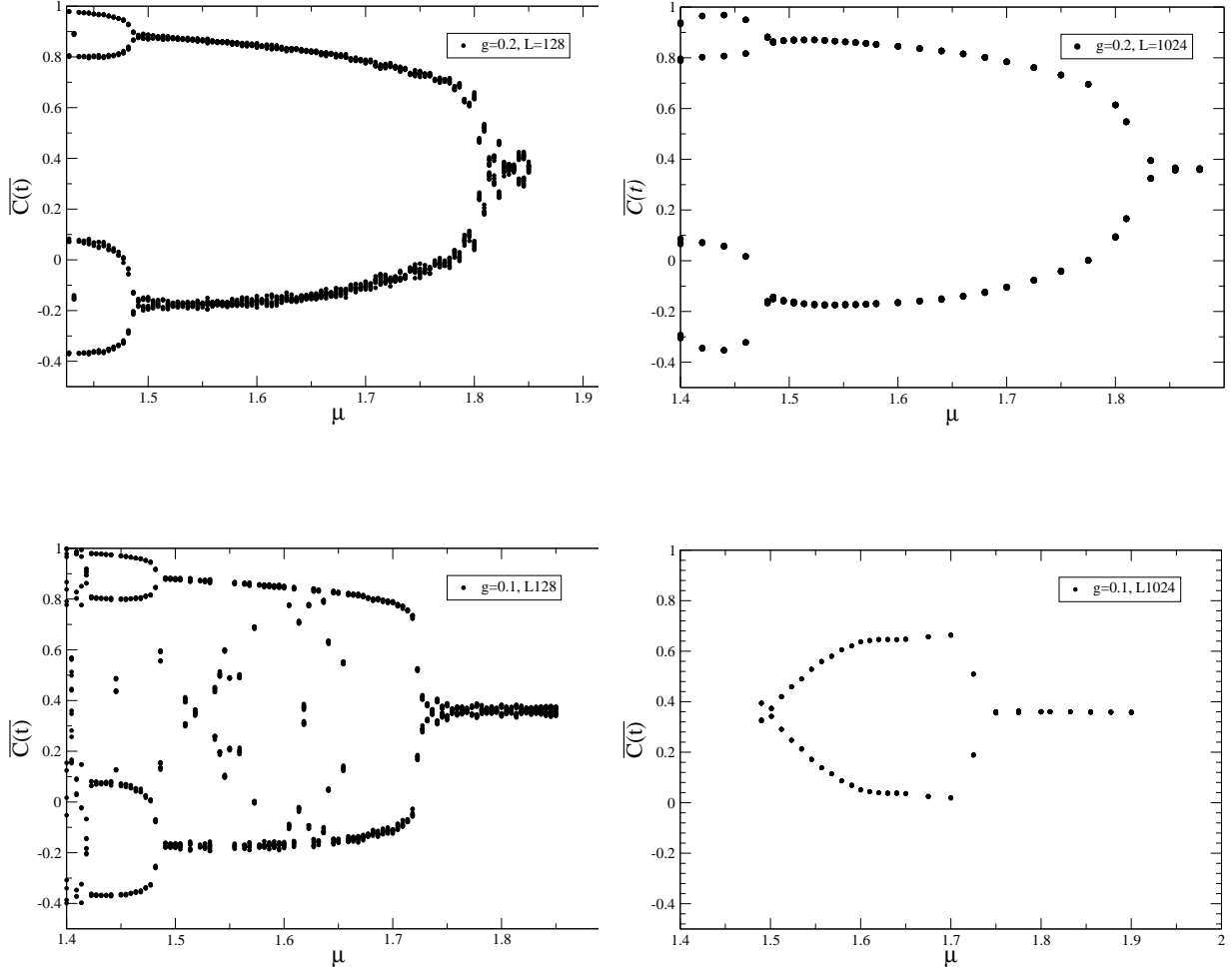


FIG. 9: The logistic CML on a regular lattice : the spatial average  $\overline{C(t)} = \frac{1}{V} \sum_x C_x(t)$  is shown as a function of  $\mu$  for the six consecutive times  $T+1, T+2, T+3, T+4, T+5, T+6$  where  $T = 10^6$  for  $L = 128$  and  $T = 10^4$  for  $L = 1024$ . System sizes and couplings are  $g = 0.2, L = 128$  (top left),  $g = 0.2, L = 1024$  (top right),  $g = 0.1, L = 128$  (bottom left),  $g = 0.1, L = 1024$  (bottom right)

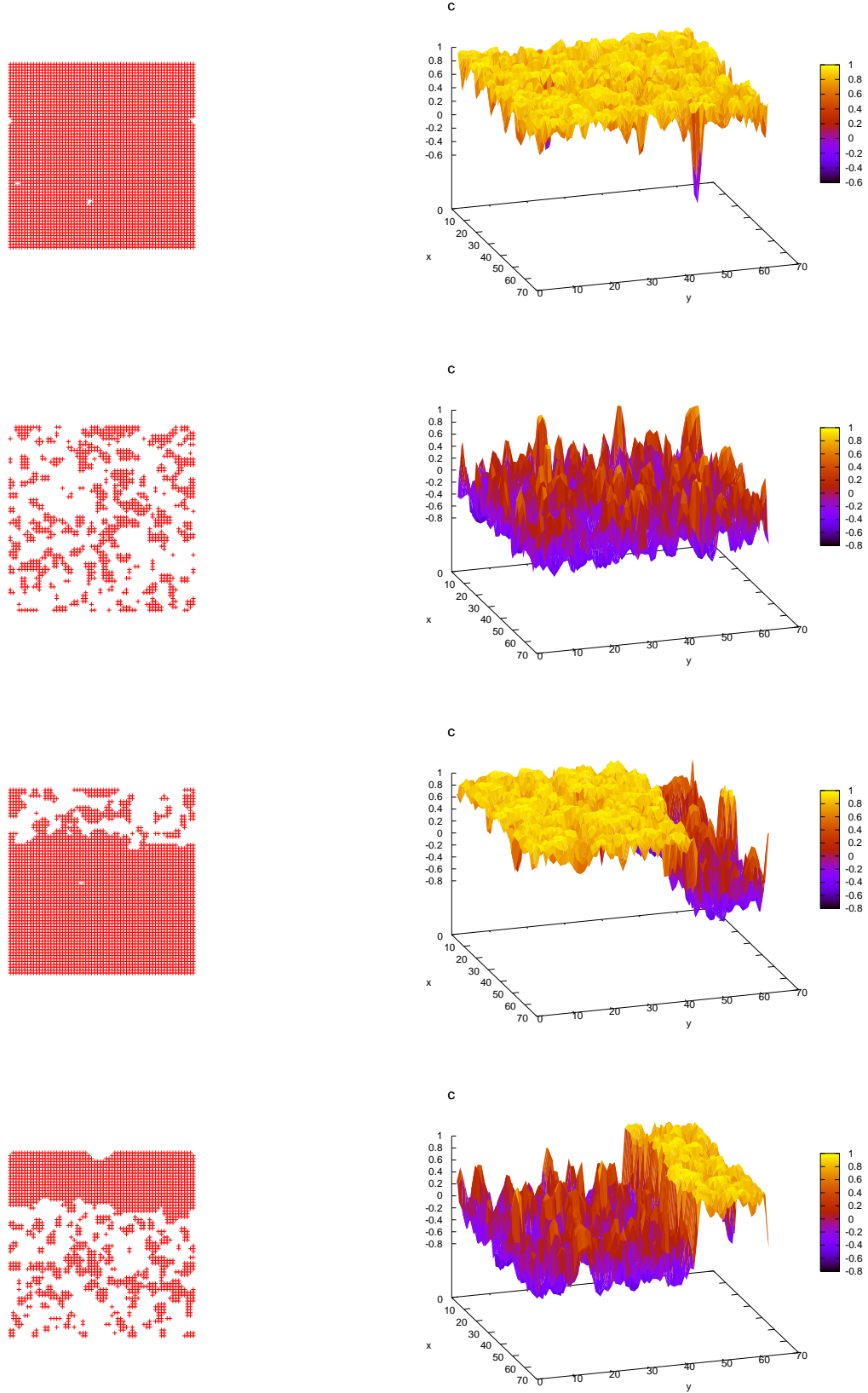


FIG. 10: (Color online) Snapshots of spin  $\sigma_x(t)$  (left) and field  $C_x(t)$  (right) for  $\mu = 1.66$ ,  $g = 0.1$ ,  $L = 64$ ,  $T = 10^6$ . Two different random initial conditions have been used for rows 1,2 and rows 3,4 respectively. Row 1 and 3 correspond to time  $T$  and rows 2 and 4 to time  $T + 1$ .



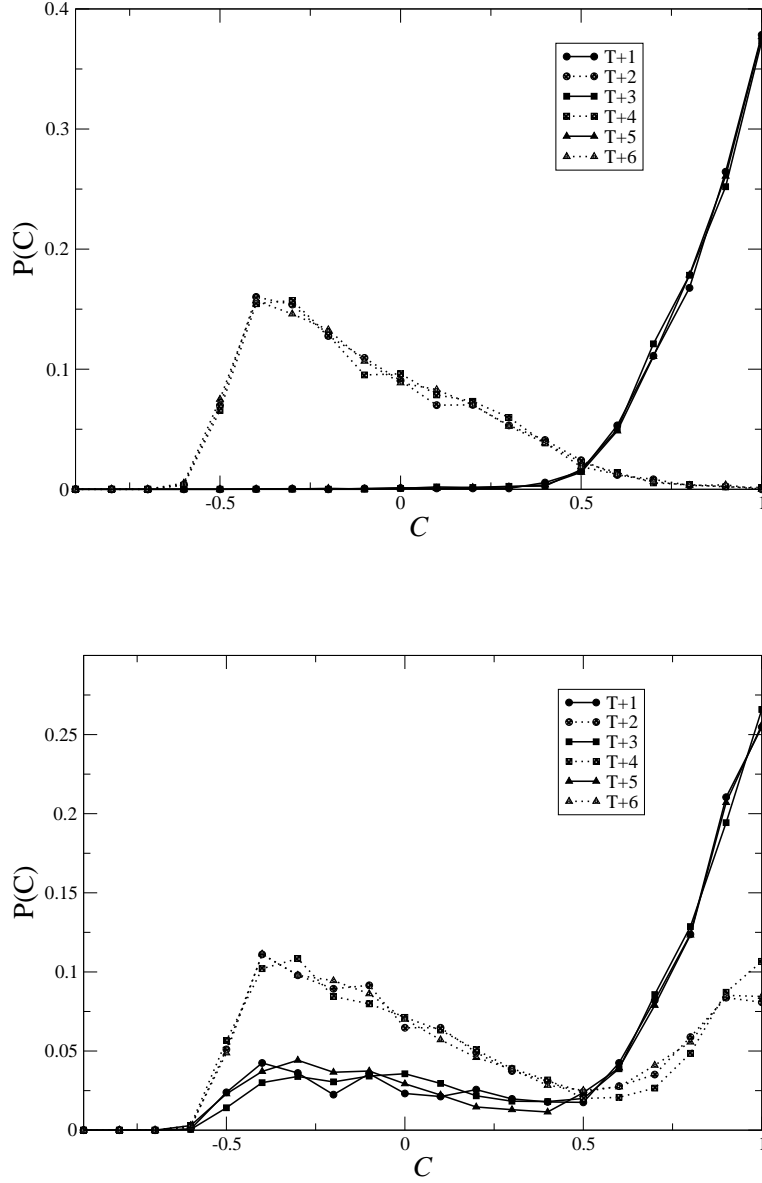


FIG. 11: Probability distribution function (PDF) of variable  $C(t)$  over the lattice for the logistic CML on a regular lattice ( $p = 0$ ) with  $g = 0.1$  and  $\mu = 1.66$ . Computations are performed with a size  $L = 64$  with top and bottom figures differing by the random initial condition. Various curves refer to six consecutive times  $T + 1$ ,  $T + 2$ ,  $T + 3$ ,  $T + 4$ ,  $T + 5$ ,  $T + 6$  with  $T = 10^6$ .

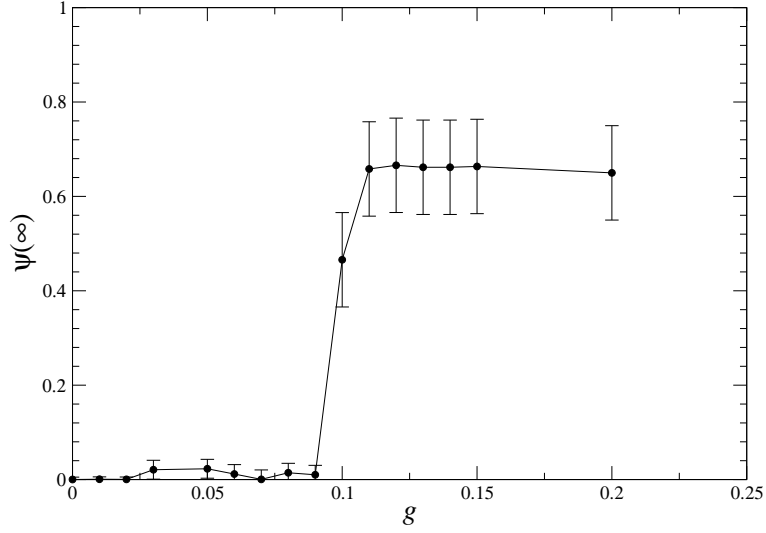


FIG. 12: Phase diagram for the undiluted logistic map: order parameter  $\psi$  vs. coupling  $g$  (see text). Here size is  $L = 1024$ ,  $\mu = 1.7$ ,  $T = 10^4$ .

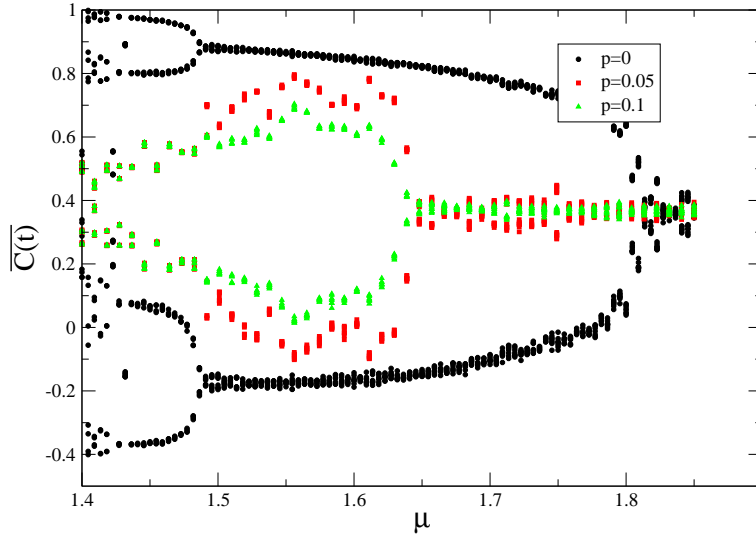


FIG. 13: (Color online) Phase diagram for the logistic CML with coupling  $g = 0.2$ , size  $L = 128$  with binary disorder  $p = 0.05$  and  $p = 0.1$ . The ordered case  $p = 0$  is shown as a comparison. Spatial average  $\overline{C(t)} = \frac{1}{V} \sum_x C_x(t)$  is displayed as a function of  $\mu$  for six consecutive times  $T + 1, T + 2, T + 3, T + 4, T + 5, T + 6$  with  $T = 4.5 \times 10^5$ .

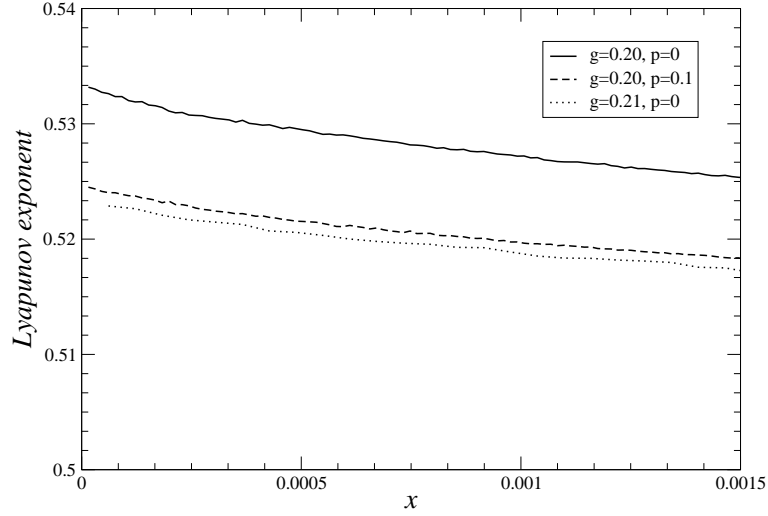


FIG. 14: The first 100 Lyapunov exponents vs. the normalized index  $x = i/L^2$  for the two-dimensional Miller-Huse CML with size  $L = 128$ . Full (resp. dotted) line refers to a regular lattice at  $\mu = 3$  and  $g = 0.20 < g_c$  (resp.  $g = 0.21 > g_c$ ). The broken line refers to a diluted case  $g = 0.20$  and  $p = 0.1$ .

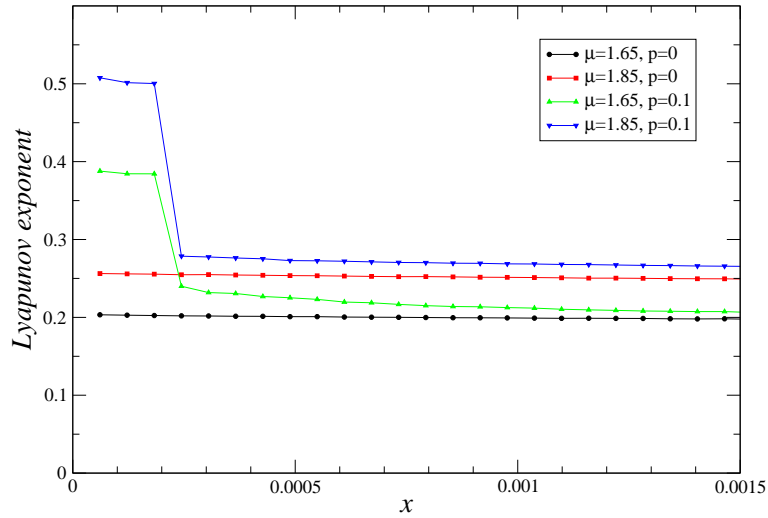


FIG. 15: (Color online) The first 100 Lyapunov exponents vs. the normalized index  $x = i/L^2$  for the logistic CML. Here the size is  $L = 128$ , coupling  $g = 0.2$  and two parameters  $\mu = 1.65, 1.85$  are considered. Two curves refer to the the undiluted ( $p = 0$ ) and diluted ( $p = 0.1$ ) logistic CML.